JGR Space Physics

RESEARCH ARTICLE
10.1029/2019JA026797

Nighttime Magnetic Perturbation Events Observed in Arctic Canada: 2. Multiple-Instrument Observations

M. J. Engebretson[1], E. S. Steinmetz[1], J. L. Posch[1], V. A. Pilipenko[1,2], M. B. Moldwin[3], M. G. Connors[4], D. H. Boteler[5], I. R. Mann[6], M. D. Hartinger[7,8], J. M. Weygand[9], L. R. Lyons[10], Y. Nishimura[10,11], H. J. Singer[12], S. Ohtani[13], C. T. Russell[9,14], A. Fazakerley[15], and L. M. Kistler[16]

[1]Department of Physics, Augsburg University, Minneapolis, MN, USA, [2]Institute of the Physics of the Earth, Moscow, Russia, [3]Department of Climate and Space Sciences and Engineering, University of Michigan, Ann Arbor, MI, USA, [4]Athabasca University Observatories, Athabasca, Alberta, Canada, [5]Geomagnetic Laboratory, Natural Resources Canada, Ottawa, Ontario, Canada, [6]Department of Physics, University of Alberta, Edmonton, Alberta, Canada, [7]Bradley Department of Electrical and Computer Engineering, Virginia Polytechnic Institute and State University, Blacksburg, VA, USA, [8]Center for Space Plasma Physics, Space Science Institute, Boulder, CO, USA, [9]Institute of Geophysics and Planetary Physics, University of California, Los Angeles, CA, USA, [10]Department of Atmospheric and Oceanic Sciences, University of California, Los Angeles, CA, USA, [11]Department of Electrical and Computer Engineering and Center for Space Physics, Boston University, Boston, MA, USA, [12]NOAA Space Weather Prediction Center, Boulder, CO, USA, [13]Johns Hopkins University Applied Physics Laboratory, Laurel, MD, USA, [14]Department of Earth Planetary and Space Sciences, University of California, Los Angeles, CA, USA, [15]Mullard Space Science Laboratory, University College London, Dorking, UK, [16]Department of Physics, University of New Hampshire, Durham, NH, USA

This article is a companion to Engebretson et al. (2019), https://doi.org/10.1029/2019JA026794.

Key Points:
- In each case study, two or three perturbation intervals occurred within a span of less than 1 hr; later intervals appeared to the north and west
- Individual perturbation events typically had a horizontal radius (center to half maximum amplitude) of ~275 km
- Events were closely associated with auroral streamers and less closely associated with substorm onsets and magnetotail dipolarizations

Supporting Information:
- Supporting Information S1
- Movie S1
- Movie S2

Correspondence to:
M. J. Engebretson,
engebret@augsburg.edu

Citation:
Engebretson, M. J., Steinmetz, E. S., Posch, J. L., Pilipenko, V. A., Moldwin, M. B., Connors, M. G., et al. (2019). Nighttime magnetic perturbation events observed in Arctic Canada: 2. Multiple-instrument observations. *Journal of Geophysical Research: Space Physics*, *124*. https://doi.org/10.1029/2019JA026797

Received 2 APR 2019
Accepted 13 AUG 2019
Accepted article online 29 AUG 2019

Abstract The rapid changes of magnetic fields associated with nighttime magnetic perturbations with amplitudes $|\Delta B|$ of hundreds of nanoteslas and 5- to 10-min periods can induce bursts of geomagnetically induced currents that can harm technological systems. This paper presents three cases of intervals of intense and complex nighttime magnetic perturbations in eastern Arctic Canada in 2015, augmented by observations from auroral imagers and high-altitude spacecraft in the nightside magnetosphere. Each case occurred within 1 hr after substorm onsets. None occurred during the main phase of a geomagnetic storm, and only the first during the early recovery phase (of a moderate storm). The cases were similar in that two or three intervals occurred in this region over a span of ~1 hr; these showed a spatial progression, in that successive intervals occurred later at more western and northern stations. During several intervals, individual peak *Bx* impulses occurred nearly simultaneously (within 1–2 min) at several stations, while during others the impulses occurred later at more western and northern stations, and during one interval they occurred later at southern stations. During both of the cases for which auroral images were available, a westward traveling surge and a poleward auroral expansion and/or poleward boundary intensification occurred, and during two events auroral streamers coincided in time and location with magnetic perturbations. These observations appear to be consistent with several earlier studies connecting nighttime magnetic perturbation events to localized auroral structures and to dipolarizing flux bundles and bursty bulk flows in the magnetotail.

1. Introduction

Large nighttime magnetic perturbation events are often observed in high-latitude magnetometer arrays. These events can induce large geoelectric fields and geomagnetically-induced currents that can have harmful effects on electrical power grids. Nighttime perturbation events have often been associated with magnetic storms and auroral substorm onsets, but several studies have suggested that other, more localized magnetospheric and/or ionospheric processes, including poleward auroral expansions and small-scale ionospheric current vortices, also may drive these events [Viljanen, 1997; Pulkkinen et al., 2003; Huttunen et al., 2002; Ngwira et al., 2015, 2018; Belakhovsky et al., 2018; Kozyreva et al., 2018, and Dimmock et al., 2019].

Eastern Arctic Canada is the only region providing dense two-dimensional ground magnetometer coverage at latitudes from the central auroral zone through contracted oval latitudes and into the near-cusp and polar cap regions. This paper presents three case studies of intense nighttime perturbation events in this region, augmented by observations from THEMIS auroral imagers and high-altitude GOES and Cluster spacecraft

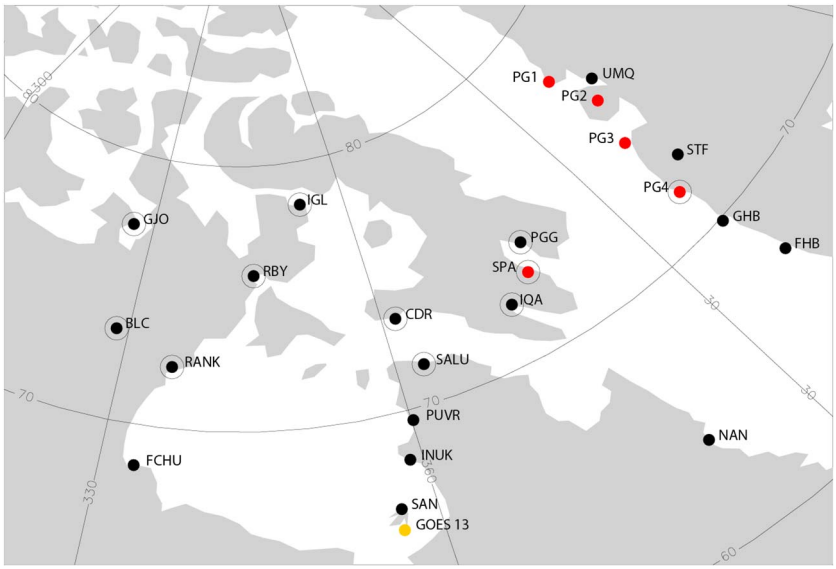

Figure 1. Map of ground magnetometer stations used for this study. The magnetic foot point of GOES 13 at 0100 UT during 2015 is shown in yellow, and the locations magnetically conjugate to Antarctic stations South Pole (SPA) and AAL-PIP PG1–PG4 are shown in red. Stations marked with large circles had max $|dB/dt| > 10$ nT/s in at least one component during the 11 November 2015 event (but at slightly different times). Selected latitude and longitude lines in geomagnetic coordinates are shown.

in the nightside magnetosphere. Section 2 introduces the instruments that provide data for this study, and section 3 presents multistation and multi-instrument observations of each event. Section 4 discusses these observations in the light of recent published work, and section 5 presents a summary of our findings. A companion paper (Engebretson et al., 2019, hereafter called Paper 1) presents a statistical survey of nighttime magnetic perturbation events recorded during 2015 at eight stations in this region, including studies of their occurrence as a function of the phase of magnetic storms and their temporal relation to substorm onsets. Paper 1 also includes a more extensive literature review of impulsive magnetic perturbations observed by ground-based magnetometers and highlights the importance of further studies of localized nightside perturbations for space weather applications.

2. Instrumentation

Magnetometer data used in this study were recorded by four arrays in Arctic Canada: MACCS (Engebretson et al., 1995), AUTUMNX (Connors et al., 2016), CANMOS (Nikitina et al., 2016), and CARISMA (Mann et al., 2008), as well as the Greenland Coastal array (http://www.space.dtu.dk/English/Research/Scientific_data_and_models/Magnetic_Ground_Stations.aspx), the conjugate AAL-PIP array in Antarctica (Clauer et al., 2014), and the fluxgate magnetometer at South Pole Station, Antarctica (Engebretson et al., 1997). Auroral images were obtained by the THEMIS all-sky white light imagers (Mende et al., 2008). High-altitude spacecraft data were obtained from GOES 13 (Singer et al., 1996), and for one event, from Cluster. The ground-based magnetometers used in this study are shown in Figure 1, and Table 1 lists their geographic and corrected geomagnetic coordinates and data sampling rates. Figure 1 also shows the magnetic foot point of GOES 13 at 0100 UT during epoch 2015, based on the default SSCweb T89C $Kp = 3$ model (Tsyganenko, 1989).

3. Observations

As described in Paper 1, full-year ground-magnetometer data sets during 2015 from eight stations were analyzed to identify all large-amplitude magnetic perturbation events. In contrast to most of the events identified in that study, which were isolated, this paper focuses on three cases of intense magnetic perturbations that consist of two or three separate activations—few-minute intervals of intense magnetic perturbations

Table 1
Magnetometer Sites Used in This Study

Array	Station	Code	Geog. Lat.	Geog. Lon.	CGM Lat,	CGM Lon.	Cadence
MACCS	Igloolik	IGL	69.3°	278.2°	77.6°	−5.0°	0.5 s
	Gjoa Haven	GJO	68.6°	264.1°	76.8°	−30.2°	0.5 s
	Repulse Bay	RBY	66.5°	273.8°	75.2°	−12.8°	0.5 s
	Pangnirtung	PGG	66.1°	294.2°	73.3°	19.8°	0.5 s
	Cape Dorset	CDR	64.2°	283.4°	72.7°	3.0°	0.5 s
	Nain	NAN	56.4°	298.3°	63.2°	22.5°	0.5 s
AUTUMNX	Salluit	SALU	62.2°	284.3°	70.7°	4.1°	0.5 s
	Puvirnituq	PUVR	60.1°	282.7°	68.9°	1.3°	0.5 s
	Inukjuak	lNUK	58.5°	281.9°	67.4°	0.0°	0.5 s
CANMOS	Iqaluit	IQA	63.8°	291.5°	71.4°	15.1°	1.0 s
	Baker Lake	BLC	64.3°	264.0°	72.9°	−28.9°	1.0 s
	Fort Churchill	FCHU	58.8°	265.9°	67.7°	−24.6°	1.0 s
	Sanikiluaq	SNK	56.5°	280.8°	65.6°	−1.8°	1.0 s
CARISMA	Rankin Inlet	RANK	62.8°	267.9°	71.7°	−22.2°	1.0 s
Greenland Coastal Array							
	Uummanaq	UMQ	70.7°	307.9°	75.7°	40.9°	1.0 s
	Kangerlussuaq	STF	67.0	309.3°	72.0°	39.6°	1.0 s
	Nuuk	GHB	64.2°	308.3°	69.3°	36.8°	1.0 s
	Paamiut	FHB	62.0°	310.3°	66.7°	38.1°	1.0 s
AAL-PIP (Antarctica)							
		PG1	−84.5°	77.2°	77.3°	37.3°	1.0 s
		PG2	−84.4°	58.0°	75.6°	39.0°	1.0 s
		PG3	−84.8°	37.6°	73.9°	36.6°	1.0 s
		PG4	−83.3°	12.3°	71.2°	36.3°	1.0 s
South Pole Station		SPA	−90.0°	—	74.5°	18.7°	1.0 s

Note. Corrected magnetic (CGM) coordinates are for epoch 2015 (using http://sdnet.thayer.dartmouth.edu/aacgm/aacgm_calc.php#AACGM).

separated by ~10-min intervals of lesser activity. They were selected without initial regard to the geophysical conditions associated with their occurrence.

For each case we first present a 3- to 4-hr plot of the heliospheric and magnetospheric context of the events. This plot includes interplanetary magnetic field (IMF) and solar wind conditions based on the OMNI time-shifted data set (available at https://cdaweb.sci.gsfc.nasa.gov), the SuperMAG SME auroral electrojet index (Newell & Gjerloev, 2011), and the vector magnetic field observed by the GOES 13 spacecraft, located at geo-synchronous orbit in the North American sector and magnetically conjugate to Hudson Bay. This plot also highlights in tan shading the time intervals during which magnetic perturbation events were observed. Second, we show stacked baseline-subtracted three-axis magnetograms of data from selected stations in the above arrays for this same time interval. Each stacked plot also includes inset values of the largest derivative values (either positive or negative) in all three magnetic field components, along with the time of their occurrence. The procedure for calculating these derivatives is presented in Paper 1. Subsequently, we present selected maps of equivalent ionospheric currents and horizontal derivatives over this region, auroral images, and magnetically conjugate high-altitude data.

3.1. Event 1: 11 November 2015 0050–0150 UT

The nighttime magnetic perturbation events during this time interval produced the largest derivatives in this data set during 2015 and were one of the most extended in space. They occurred 4 days after a $Dst = -89$ magnetic storm, and ~11 hr after a moderate $Dst = -58$ magnetic storm. During the events, $Dst = -27$ nT.

Figure 2b shows that the north-south (Bz) component of the IMF was on average near −2 nT from 0000 to 0115 UT, but with a brief positive excursion at 0018 UT and a longer excursion beginning near 0045 UT. After 0117 UT it remained mostly positive near +2 nT. Increases in IMF Bz near 0045 and 0115 UT coincided approximately with large increases in the SME index (Figure 2e) and with substorm onsets at 0044 UT (65° MLAT, 5.17 MLT) and 0107 UT (72°, 18.9 MLT) listed in the SuperMAG substorm database. The east-west (By) component of the IMF shown in Figure 2a, the solar wind flow speed (Figure 2c),

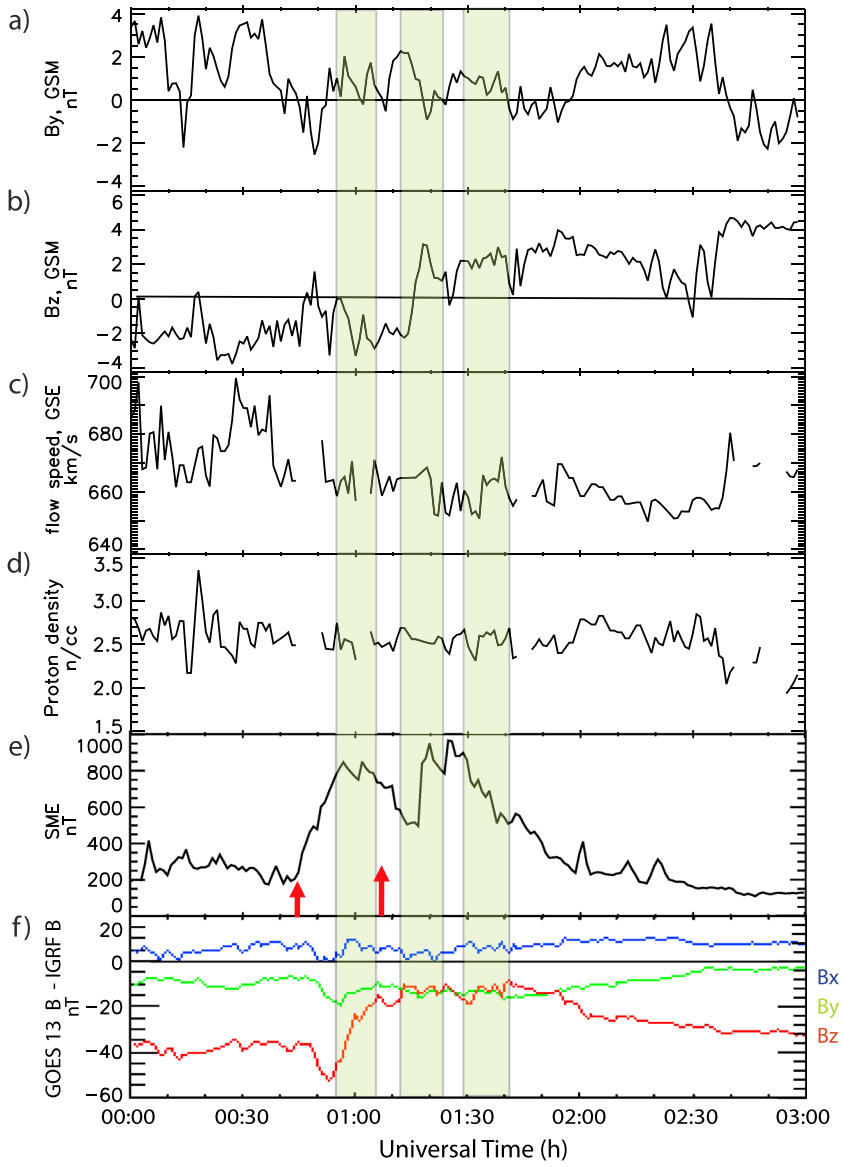

Figure 2. OMNI data (panels a–d), the 1-min SME index (panel e), and GOES 13 magnetic field data (panel f) from 0000 to 0300 UT 11 November 2015. Panels (a) and (b) show the east-west and north-south components of the interplanetary magnetic field (*By* and *Bz*, respectively), panel (c) shows the solar wind flow speed (Vsw), and panel (d) shows the solar wind proton density (Nsw), all propagated in time to the bow shock. SuperMAG substorm onset times are indicated by red arrows at the bottom of panel (e). Panel (f) shows the difference between the observed magnetic field at geostationary orbit and the IGRF model field (in solar magnetic coordinates) for three field components: *Bx* (blue), *By* (green), and *Bz* (red). The time intervals during which magnetic perturbation events were observed are highlighted in tan shading.

and the solar wind proton density (Figure 2d) exhibited modest variations, but these evidently had little effect on the SME index (Figure 2e). SuperMAG substorm onset times are indicated by red arrows at the bottom of Figure 2e. A sharp rise in the *Bz* component of the magnetic field in SM coordinates measured at GOES 13 near 0100 UT (Figure 2f) indicates a dipolarization of the nightside magnetic field at geosynchronous orbit, in the same local time sector as the ground-based magnetometer array, again consistent with the substorm activity indicated by the SME index. Figure 2 shows that the three intervals of magnetic perturbations occurred when the SME index was enhanced and within 1 hr of the first substorm onset and the dipolarization at GOES 13, but they do not show any consistent temporal relation to the onsets or the dipolarization.

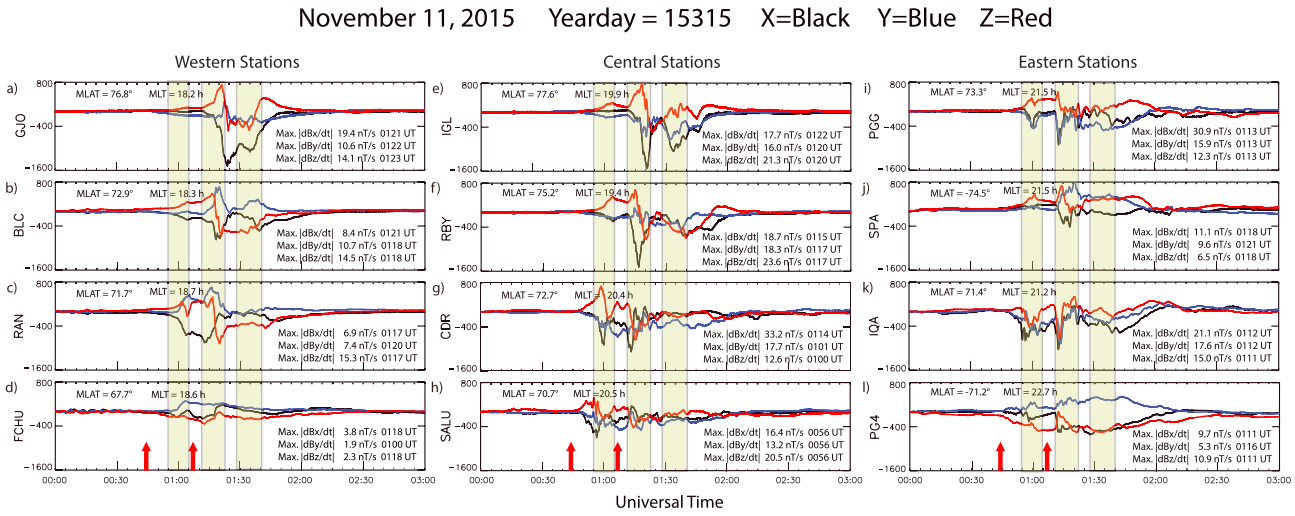

Figure 3. Three-axis magnetograms of 12 magnetometer stations in Arctic Canada from 0000 to 0300 UT 11 November 2015, grouped horizontally by longitude (and magnetic local time) and vertically by magnetic latitude. The north-south (*X*) component trace is shown in black, the east-west (*Y*) component trace in blue, and the vertical (*Z*) trace in red. At the lower right of each panel are shown the largest derivative values (either positive or negative) in all three magnetic field components that occurred during the event, along with the time of their occurrence. SuperMAG substorm onsets at 0044 and 0107 UT are indicated by red arrows at the bottom of panels (d), (h), and (l). The time intervals during which magnetic perturbation events were observed are highlighted in tan shading.

Figure 3 shows magnetograms from midnight to 0300 UT from stations with max |d*B*/d*t*| >10 nT/s (except for Fort Churchill), arranged horizontally by longitude (and magnetic local time) and vertically by magnetic latitude. Magnetic local times at each station were calculated for 0100 UT.

Magnetometer traces at all sites were relatively flat until 0045 UT, and from then until after 0200 UT, variations were observed at all the stations shown. Three intervals of perturbation event activity highlighted in Figure 2 are visible in Figure 3 between 0055 and 0142 UT. Appearing first at each station were gradual changes in each component: At most stations the *Bx* component dropped, but excursions could occur in either direction in the *By* and *Bz* components. These variations correspond to substorm bays. The much larger peaks that grew and decayed within a time span of 5–10 min and were often most prominent in the *Bx* component are the perturbation events. The events were again most often unipolar in *Bx* but could be either unipolar or bipolar in *By* and *Bz*.

In the first interval (0055–0105 UT), a large negative peak in *Bx* first appeared at Iqaluit at 0055 UT (Figure 3k) and was quickly followed by a negative peak in *Bx* at Salluit (Figure 3h). At 0100 UT negative peaks in *Bx* and *By* appeared at Pangnirtung (Figure 3i), and large peaks in *Bx* and *Bz* appeared at Cape Dorset. Weaker perturbations appeared at stations farther north and west in the ensuing minutes, until ~0105 UT (Repulse Bay, Figure 3f; Fort Churchill, Figure 3d; Rankin Inlet, Figure 3c; and Baker Lake, Figure 3b). During the second interval, peaks appeared at all of the stations shown between 0112 and 0124 UT, generally occurring earlier at the more southern stations (Iqaluit simultaneous with Pangnirtung) but progressing in time northward from Salluit to Cape Dorset to Repulse Bay to Igloolik and progressing from Fort Churchill to Rankin Inlet to Baker Lake to Gjoa Haven. During the third interval, weaker peaks appeared most clearly at the central and western stations between 0129 and 0142 UT. In contrast to the other two cases shown, the peaks within each interval were not simultaneous but rather showed a mostly northward temporal progression. The perturbations at the two Antarctic stations, South Pole and AAL-PIP PG4 (Figures 3j and 3l), do not follow this trend, possibly because the mappings of these stations to the conjugate hemisphere are imprecise.

The maximum derivative values in each component usually but not always occurred within 1–2 min of the associated peak perturbations. The two largest derivatives were 33.2 nT/s at Cape Dorset and 30.9 nT/s at Pangnirtung, both in the *X* component, but at 6 of the 11 stations, the largest derivatives were observed in the *Z* component.

The spherical elementary current systems (SECS) technique developed by Amm and Viljanen (1999) uses vector magnetometer data from an array of ground stations to infer ionospheric equivalent vector

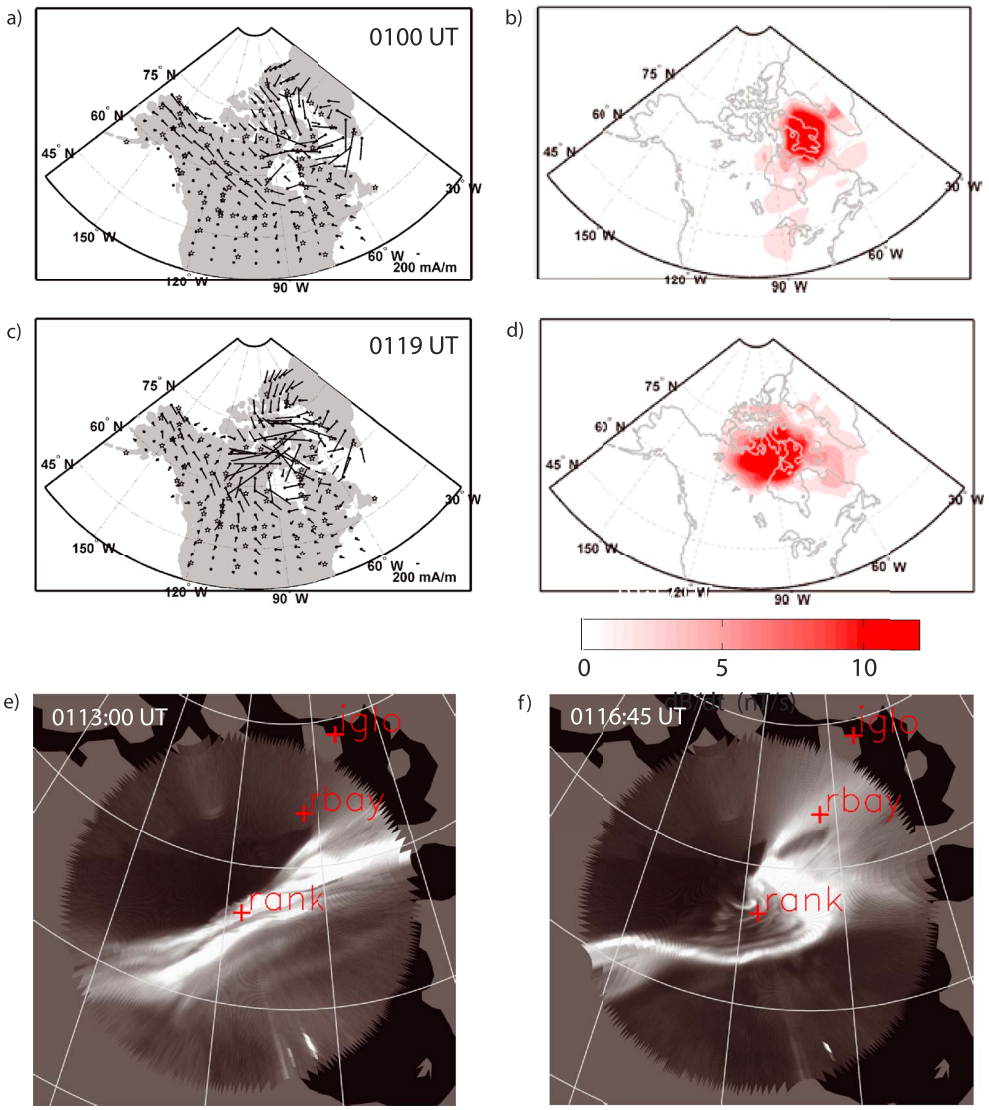

Figure 4. (a–d) Equivalent ionospheric current vectors (panels a and c) and contour maps of the horizontal derivative of the magnetic field above Arctic Canada and western Greenland (panels b and d), calculated by applying the Spherical Elementary Current Systems technique to 10-s cadence vector magnetometer data. The value of the derivative is coded according to the color bar below panel (d). Panels (a) and (b) show values at 0100 UT, and panels (c) and (d) show values at 0119 UT, during the 11 November 2015 magnetic perturbation event shown in Figure 3. (e and f) Auroral images obtained by the all-sky imager at Rankin Inlet at 0113 and 0116:45 UT, respectively. The locations of Rankin Inlet, Repulse Bay, and Igloolik are denoted by red crosses.

currents, field-aligned currents, and derivatives of the horizontal magnetic field (SQRT($(dBx/dt)^2+(dBy/dt)^2$) in the region covered by the measurements. Weygand et al. (2011) implemented the SECS technique to produce maps of such currents over North America and Greenland, using 10-s cadence data from 11 ground arrays: AUTUMNX, CARISMA, CANMOS, DTU, Falcon, GIMA, MACCS, McMAC, STEP, THEMIS, and USGS. SECS plots of the above quantities were produced at a 1-min cadence between 0045 and 0145 UT on this day.

Figures 4a–4d show equivalent current and horizontal derivatives of *B* at two times when intense horizontal derivatives were prominent. At 0100 UT a narrow channel of strong westward equivalent currents (up to ~1,000 A) centered over southern Baffin Island (Figure 4a) was embedded within a large region of horizontal derivatives >10 nT/s (red color in Figure 4b) over southern and central Baffin Island. The large perturbations and derivatives at Cape Dorset (Figure 3g) and smaller perturbation peak at Pangnirtung (Figure 3i) are

consistent with these larger-scale patterns. By 0119 UT the equivalent currents had intensified over much of the region, and a narrow channel of the most intense currents was centered northwest of Hudson Bay (Figure 4c). An even larger region of >10-nT/s horizontal derivatives was at this time also centered northwest of Hudson Bay (Figure 4d), consistent with the larger perturbations and peak derivatives observed at IGL, BLC, RAN, and FCHU between 0118 and 0120 UT.

An auroral all-sky imager at Rankin Inlet provided observations of the aurora associated with the magnetic impulse over RBY. Movie S1 in the supporting information shows the auroral emissions recorded by the Rankin Inlet imager during the interval from 0050 to 0130 UT on 11 November 2015, from which the images in Figures 4e and 4f were taken.

Earlier images from the THEMIS array (not shown) indicated that a westward traveling surge moved over the RANK latitude stations, producing a magnetic depression in the *X* component that began at IQA near 0054 UT, at CDR near 0058 UT, and RANK near 0102 UT. The arcs near the head of the surge then turned more toward a southwest to northeast orientation, leading to a bright arc along a highly tilted auroral poleward boundary that was stationary between 0110 and 0113 UT (Movie S1 and Figure 4e). A strong poleward boundary intensification (PBI) formed along this arc beginning at 0114 UT, becoming a vortex with a strong north-south oriented arc (known as a streamer) that reached to RBY from ~0116 to 0118 UT (Figure 4f). This corresponded well to the sharp *X* component drop at RBY at this time shown in Figure 3f. Note that viewing and projection are limited near the edge of the field of view, and there is some background lighting to the north. Thus, the aurora is a bit obscured and probably not precisely projected right at RBY. But given the *X* component at RBY, that arc/streamer (which seems to be along a distorted oval poleward boundary) must have gone nearly directly overhead. The RBY *Z* component going through 0 near 0116 UT is also consistent with an overhead arc crossing. The IGL magnetometer data (Figure 3e) suggests that the same form evolved at IGL a few minutes later, but no auroral observations were available there.

3.2. Event 2: 5 February 2015 0400–0440 UT

The magnetic perturbation events during this time interval occurred 3 days after a weak storm (min $Dst = -40$) and showed a primarily westward temporal progression. A substorm onset was identified near Nuuk, Greenland (70° MLAT, ~1 hr MLT east of Iqaluit) at 0400 UT (1:26 MLT). During the event, $Dst = -4$.

Figure 5 shows that changes in several upstream variables (increases in IMF *By* and *Bz*, small fluctuations in the solar wind flow speed, and large increases in the solar wind proton density) all coincided with the substorm onset and an increase in the SME index. A sharp rise in the *Bz* component of the magnetic field at GOES 13 near 0415 UT (Figure 5f) again indicates a dipolarization of the nightside magnetic field at geosynchronous orbit, in the same local time sector as the ground-based magnetometer array. The three intervals of magnetic perturbations again occurred during times when the SME index was enhanced but again showed no consistent temporal relation to the substorm onset or the dipolarization at GOES 13.

The five magnetograms in Figure 6 show the stations with largest derivatives on this day, arranged in order of MLT with the westernmost station (earlier MLT) at the top. Two of the three intervals of activity highlighted in Figure 5 were of shorter duration than those in the first event. This reflects the near simultaneity of the largest minima in the *Bx* component during each interval: Minima in *Bx* occurred near 0408 UT at IQA and PGG (Figures 6d and 6e), near 0417 UT at CDR, IQA, and PGG (Figures 6b, 6d, and 6e), and near 0432 UT at RBY, CDR, and IQA (Figures 6a, 6b, and 6d).

The largest derivatives occurred at PGG at 0417 UT and at CDR at 0432 UT, in the *X* component. The maximum derivatives in each component again (except at SALU) occurred within 1–2 min of the associated peak perturbations. Thus, in this example there was a northward progression of perturbation events with time, but within each interval the perturbations and maximum derivatives were nearly simultaneous.

SECS horizontal derivative maps during this interval showed the greatest intensities at two times, 0420 and 0431 UT (Figure 7). At 0420 UT a region with derivatives up to 6 nT/s was centered over southern Baffin Island (Figure 7a), consistent with the large perturbations at PGG, IQA, and CDR, and at 0431 UT a

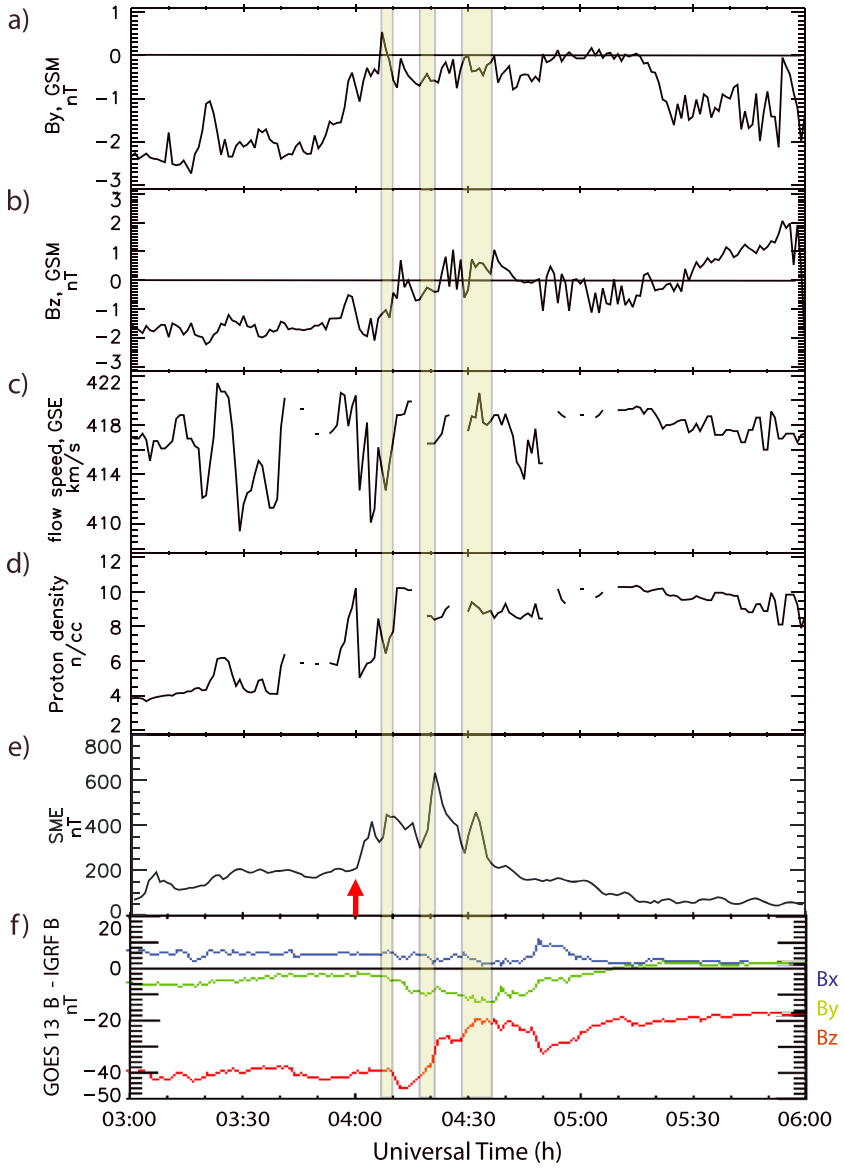

Figure 5. OMNI data (panels a–d), the 1-min SME index (panel e), and GOES 13 magnetic field data (panel f) from 0300 to 0600 UT 5 February 2015, as in Figure 2. A substorm onset at 0400 UT is indicated by the red arrow at the bottom of panel (e).

smaller region with a slightly weaker maximum appeared over southwestern Baffin Island, northern Quebec, and north of Hudson Bay (Figure 7b), consistent with the perturbations at IQA, SALU, CDR, and RBY.

Moonlight obscured the auroral signatures during these perturbation events, and all-sky imager array coverage did not extend over Baffin Island, so no aurora could be observed over CDR and PGG. A poleward expansion started at about 0415 UT over Hudson Bay, but it was mostly outside the imager field of view. Later a streamer appeared northeast of Rankin Inlet at 0427 UT (at the eastern edge of the imager's field of view in Figure 7c) and moved northward over Repulse Bay (Figures 7d and 7e, at 0430 and 0431:30 UT) before fading by 0433 UT (Figure 7f). The appearance, movement, and disappearance of this streamer are consistent with the perturbation event observed at RBY (Figure 6a) and coincide with the western edge of the region of most intense derivatives shown in Figure 7b. Movie S2 is a movie of the auroral emissions recorded by three auroral imagers (at Rankin Inlet, Sanikiluaq, and Kuujjuaq) during the interval from 0345 to 0445 UT on 5

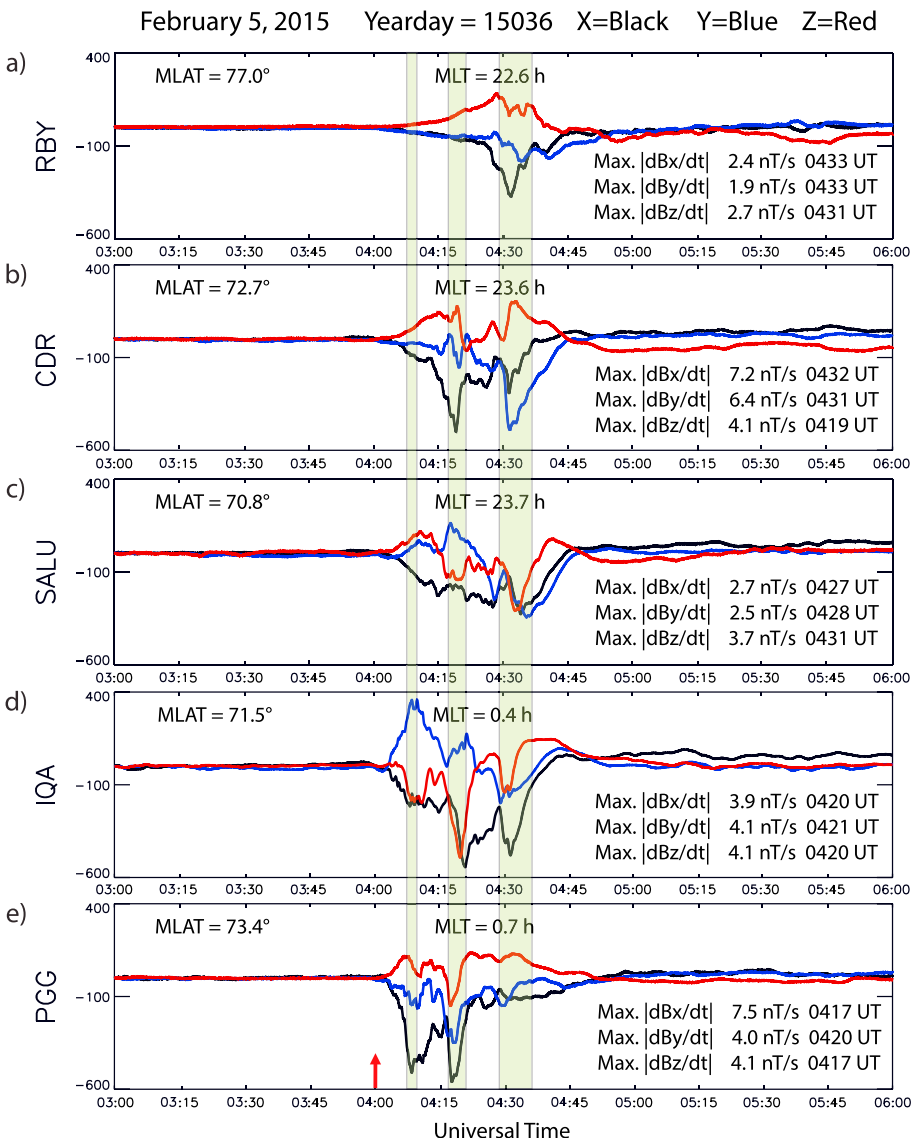

Figure 6. Three-axis magnetograms of five magnetometer stations in Arctic Canada from 0300 to 0600 UT 5 February 2015, as in Figure 3. Panels are arranged in order of magnetic local time, with the westernmost station (earlier MLT) at the top. A substorm onset at 0400 UT is indicated by the red arrow at the bottom of panel (e).

February 2015, from which these images were taken. The movie also shows a streamer coming from the direction of PGG and oriented to the southwest over Iqaluit (which is located at the northern edge of the field of view of the eastern imager) between 0407 and 0409 UT, which corresponds in time to the *X* component drops at PGG (Figure 6e) and IQA (Figure 6d) at this time, as well as a similar but more short-lived streamer near 0413 UT.

3.3. Event 3: 9 October 2015 2120–2240 UT

The perturbation events during this time interval, involving the occurrence of two relatively localized impulses within a span of ~30 min, occurred 2 days after a moderate storm (min *Dst* = −124). The second of these events, near 2200 UT, occurred almost simultaneously (within 1–2 min) over a ~650-km range, from Salluit to Pangnirtung, showing little or no spatial progression. Substorm onsets were identified east of the southern tip of Greenland (64° MLAT), ~5 hr MLT east of Iqaluit, at 2052 UT (23:22 MLT) and 2114 UT (23:43 MLT). During the event *Dst* = −48 nT.

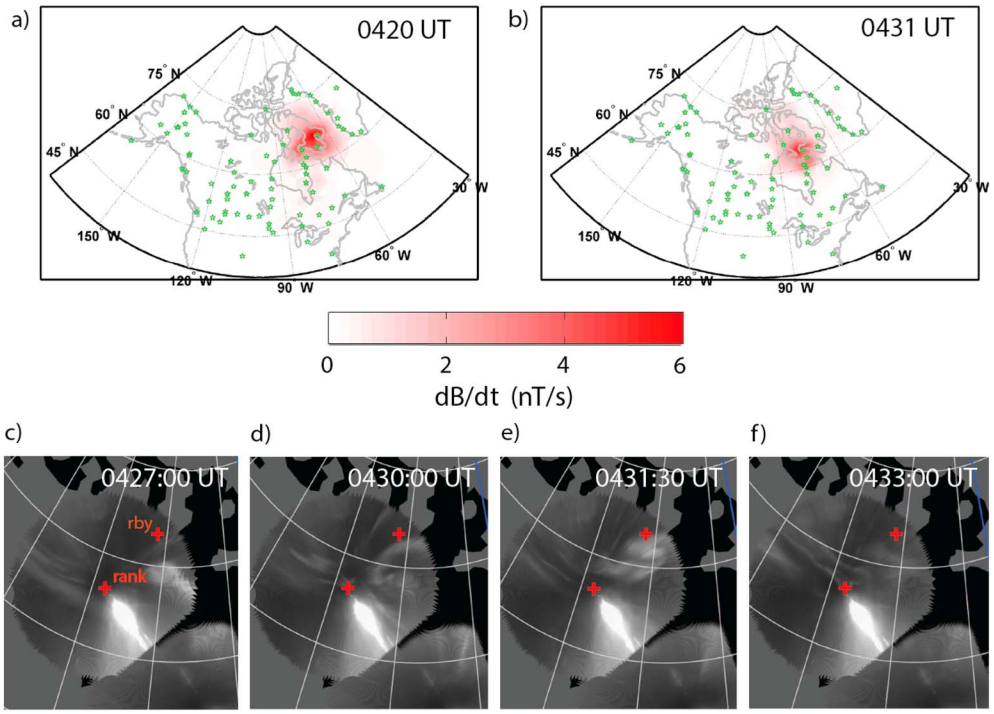

Figure 7. (a and b) Contour maps of the horizontal derivative of the magnetic field above Arctic Canada and western Greenland calculated by applying the SECS technique to 10-s cadence vector magnetometer data at 0420 UT (panel a) and 0431 UT (panel b), during the 5 February 2015 magnetic perturbation event shown in Figure 6. (c–f) Auroral images obtained by the all-sky imager at Rankin Inlet at 0427, 0430, 0431:30, and 0433 UT, respectively. The locations of Rankin Inlet and Repulse Bay are denoted by red crosses.

Figure 8b shows that IMF *Bz* was mostly negative from 2000 to 2200 UT but exhibited several rapid rises to or slightly above 0: The first two, near 2050 and 2114 UT, coincided closely with substorm onsets, and the third, near 2150 UT, coincided with the onset of the second event. Large variations in IMF *By* (Figure 8a) did not correlate closely with those in IMF *Bz* or with the relatively small variations in solar wind flow speed (Figure 8c) and proton density (Figure 8d). Increases in the SME index (Figure 8e) coincided approximately with the substorm onset at 2052 UT and the third rapid rise in IMF *Bz* near 2150 UT. The *Bz* magnetic field component at GOES 13 (Figure 8f) varied widely during this interval but indicated two dipolarizations roughly coincident with increased SME index values, and as will be shown in Figure 9, in this case in good temporal agreement with the two intervals of largest perturbations in the ground magnetic field data. Neither perturbation interval was close in time to the substorm onsets.

The five magnetograms in Figure 9 show the stations with largest derivatives, arranged in order of MLAT. The most poleward station (at South Pole, Antarctica) observed larger amplitude perturbations than any of the more western stations in the Northern Hemisphere. No Antarctic AAL-PIP data (conjugate to western Greenland) were available for this day.

The two intervals of perturbation event activity highlighted in Figure 9 were of intermediate duration. The first events occurred at IQA (Figure 9d) and more weakly at PGG and CDR (Figures 9b and 9c), at 2133 UT, and slightly later, at 2139 UT, at IQA and farther west at SALU (Figure 9e). The second interval of events began almost simultaneously at PGG, CDR, IQA, and SALU (Figures 9b–9e) near 2155 UT, and at SPA (Figure 9a) in Antarctica at 2–3 min later, but was extended in time in at least one component at each station. Weaker events extended from ~2215 to beyond 2230 UT at all stations, and steadier electrojet activity was evident at all stations until past 2400 UT. The largest derivatives at each of the five stations occurred during the second interval within 2 min of 2159 UT.

SECS horizontal derivative maps were consistent with the magnetometer data (Figure 10). A moderate amplitude intensification at 2135 UT was centered over southeast Baffin Island and western Greenland

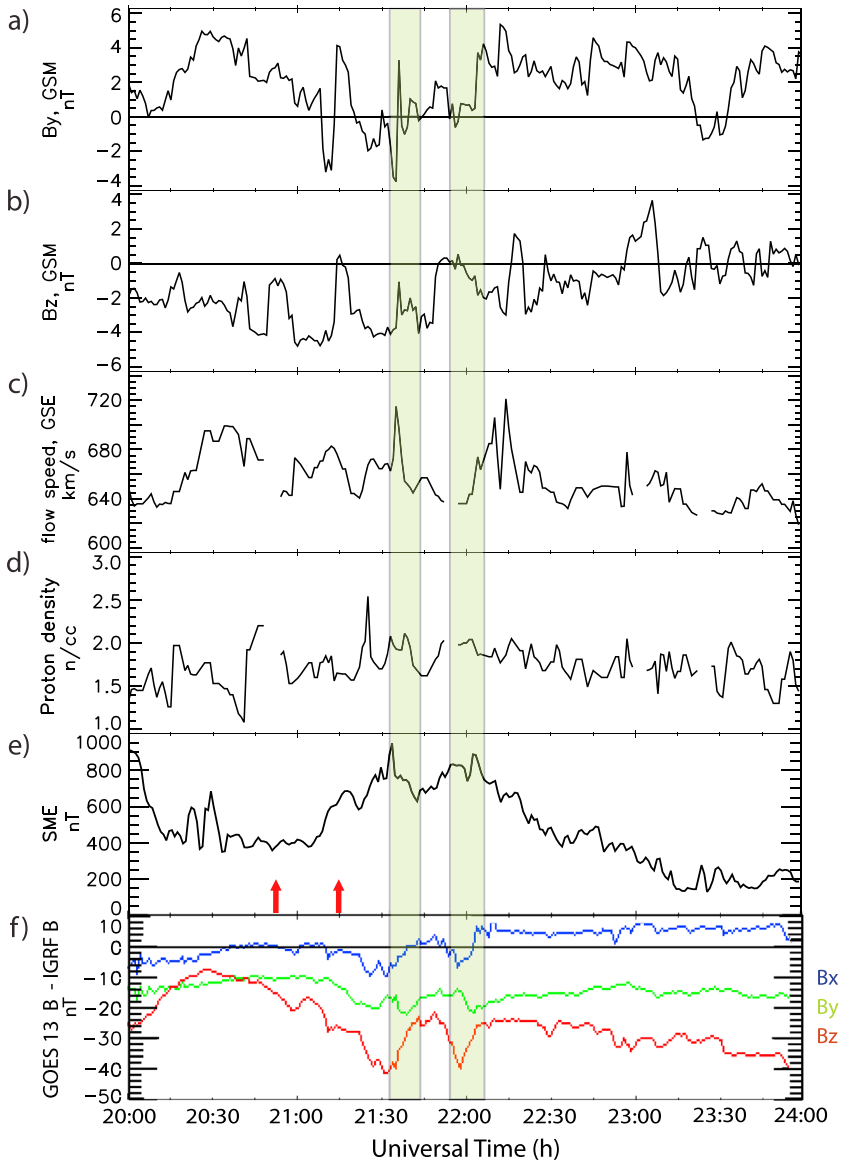

Figure 8. OMNI data (panels a–d), the 1-min SME index (panel e), and GOES 13 magnetic field data (panel f) from 2000 to 2400 UT 9 October 2015, as in Figure 2. Two substorm onsets are indicated by the red arrows at the bottom of panel (e).

(Figure 10a) consistent with the first perturbation event at IQA and impulses at FHB and GHB in western Greenland (not shown). A second moderate intensification at 2139 UT was localized over northern Quebec (Figure 10b), consistent with the first event at SALU. The third, strongest intensification at 2159 covered the southern half of Baffin Island and reached nearly to northern Quebec (Figure 10c), consistent with events at PGG, CDR, IQA, and SALU. These events occurred in daylight, so imager data were not available.

The foot point of the Cluster spacecraft, located in the premidnight magnetotail near 10 R_E, moved from Greenland westward over Arctic Canada during this event. Figure 11a shows the mapped Northern Hemisphere ground tracks of Cluster using an ensemble of magnetic field models provided by SSCWeb: the default T89c $Kp = 3$ model (Tsyganenko, 1989) and six others for which magnetic activity values were selected to match the conditions of this event: T89c $Kp = 4$, T87Wd (Tsyganenko, 1987) $Kp = 4$, and T96 (Tsyganenko, 1996) using Psw = 1.7 nPa, $Dst = -42$ nT, IMF $By = 0$ nT, and four different values of IMF Bz: 0, −1.0, −2.0, and −3.0 nT. The models placed the foot point of Cluster at 2200 UT slightly southeast

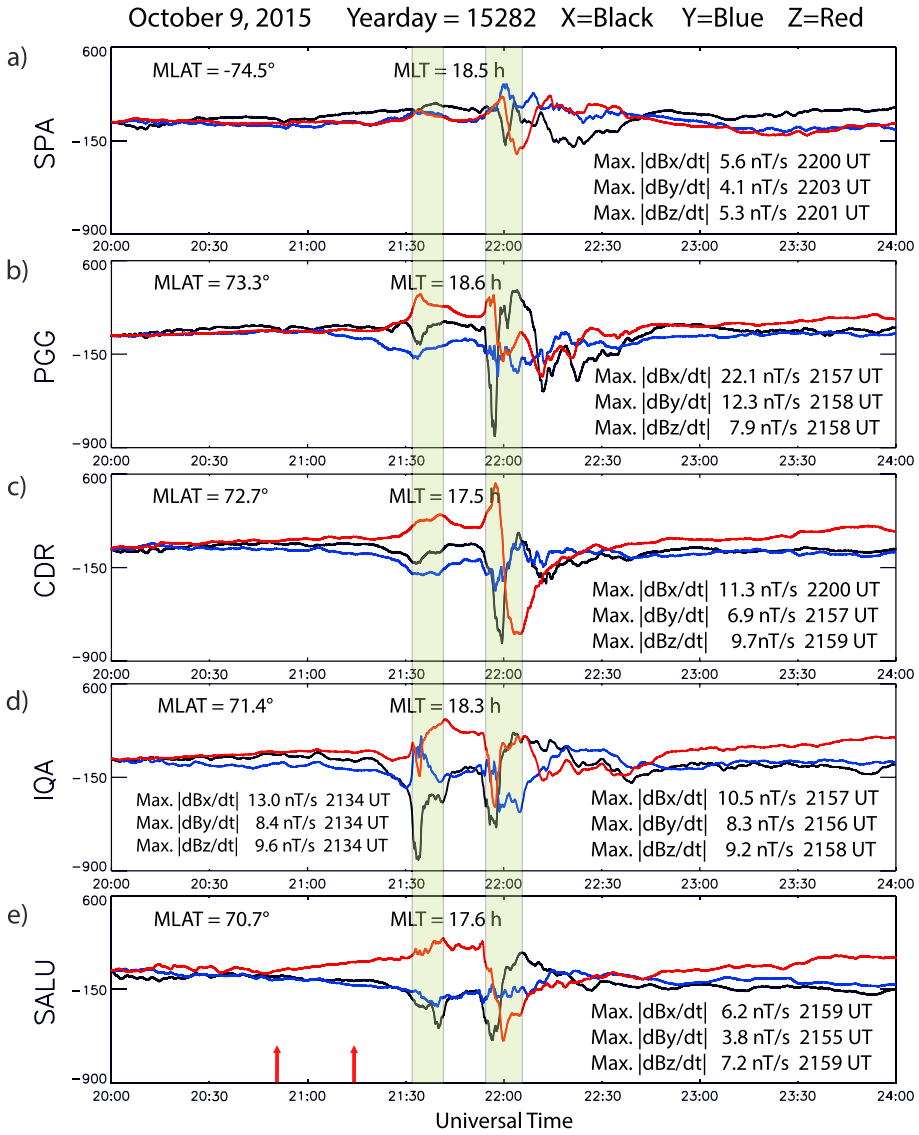

Figure 9. Three-axis magnetograms of five magnetometer stations in Arctic Canada from 2000 to 2400 UT 9 October 2015, as in Figure 3. Panels are arranged in order of magnetic latitude, with the northernmost station at the top. Substorm onsets are indicated by the red arrows at the bottom of panel (e).

of PGG when mapped by the T89c3 and T89c4 models, and slightly southeast of Iqaluit at slightly different latitudes when mapped using the four T96 models.

Energetic electron data from the Plasma Electron and Current Experiment (Johnstone et al., 1997) are shown in Figures 11b–11d, and energetic ion data from the Cluster Ion Spectroscopy (CIS) instrument (Rème et al., 2001) are shown in Figure 11e. Both instruments observed multiple crossings between the magnetotail lobe and the plasma sheet during this 4-hr interval, and magnetic field data from the Fluxgate Magnetometer (Balogh et al., 2001) exhibited a dipolarization from 2120 to 2130 UT and a sharp field reconfiguration near 2155 UT, during one of the lobe/plasma sheet crossings (Figure 11f). Both the dipolarization and the field reconfiguration coincided with relative maxima in the total pressure (the sum of plasma pressure and magnetic field pressure, not shown), which are often used as indicators of substorm onsets in the Cluster data (Kistler et al., 2006; Liu et al., 2013). The dipolarization preceded the first perturbation event and the first dipolarization observed at GOES 13 by ~10 min. The subsequent reconfiguration preceded the second dipolarization at GOES 13 and the second event by ~5 min.

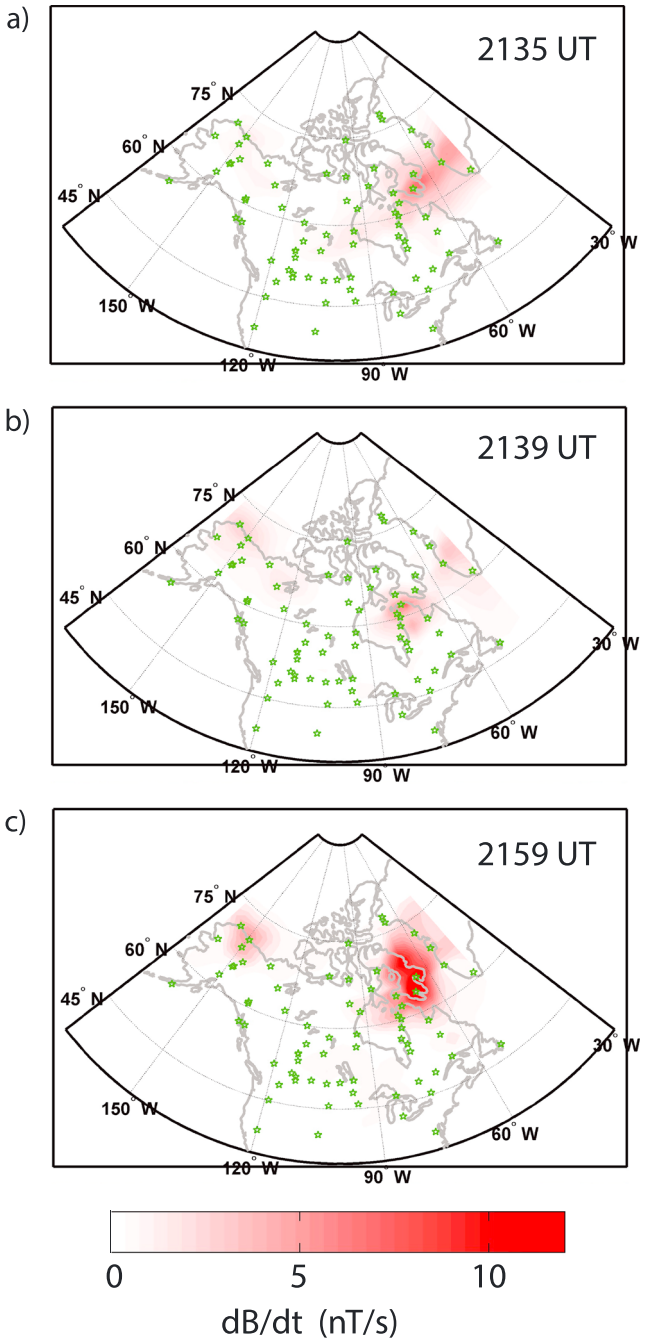

Figure 10. Contour maps of the horizontal derivative of the magnetic field above Arctic Canada and western Greenland calculated by applying the spherical elementary current systems technique to 10-s cadence vector magnetometer data at 2135 UT (panel a), 2139 UT (panel b), and 2159 UT (panel c), during the 9 October 2015 magnetic perturbation event shown in Figure 9.

4. Discussion

This study has presented three examples of two to three intervals of nighttime magnetic perturbation events observed by a number of ground magnetometers in Arctic Canada, in each case complemented by contour maps of the horizontal derivatives of the magnetic field overhead of a much larger region of North America, produced by a SECs analysis. Two cases were accompanied by auroral images showing auroral streamers over one of these magnetometer stations, and the third was accompanied by particle and magnetic field observations from Cluster.

Each of these examples followed one or more substorm onsets (with various and often large time delays). Most of the event intervals in each case were associated with increased levels of the SME index, and some were temporally associated with dipolarizations observed at GOES 13 or deeper in the magnetotail at Cluster.

The three cases were similar in two ways: (1) Two or more intervals of temporally associated events occurred in each, and (2) the intervals occurred with greatest intensity progressively later at the more western and northern stations. As described below, the cases also showed differences in two ways: (1) their spatial scale and (2) the timing of individual events within the intervals.

1. On 11 November large perturbation events were embedded within a region of magnetic disturbances that continued more than 1 hr in UT and covered a large two-dimensional area: over 3 hr in MLT (the limit of the available longitudinal coverage) and 6° in MLAT. On 5 February strong disturbances lasted ~1 hr UT, and the region of largest events extended 2 hr in MLT. On 9 October strong disturbances lasted ≥3 hr UT; the region of largest events was narrow in MLT (1.1 hr), and the MLAT range was 2.6° (the limit of the available data on this day).
2. On 11 November the peak *Bx* impulses within each interval generally occurred later at northern and western stations. Within the second and third intervals on 5 February, the peak *Bx* impulses were nearly simultaneous (within 1–2 min) at most stations but occurred later at the two lower-latitude stations (SALU and IQA). On 9 October the peak *Bx* perturbations within each interval were also nearly simultaneous.

In the following subsections we review earlier studies that are consistent with the observations reported here.

4.1. Connections to Earlier Auroral Studies

During both of the case studies for which auroral images were available, magnetic activity was generally associated with westward traveling surges, known to be regions with strong, localized currents and sharp conductance gradients (Amm et al., 2001; Ngwira et al., 2018), and the largest nightside magnetic perturbations were closely connected to poleward auroral expansions and one or more tilted poleward boundary arcs and/or auroral streamers. Lyons et al. (2013) analyzed 14 substorm events during 2007 selected solely on the basis of availability of good auroral imager coverage over North America and found abrupt auroral zone H decreases at stations near a streamer at times varying from just a few minutes to well over a half hour after substorm onset if there was a prolonged period of streamers.

An earlier substorm study by Lühr et al. (1998) based on observations over Scandinavia using magnetometers, auroral imagers, and the EISCAT radar noted a close association between a westward traveling

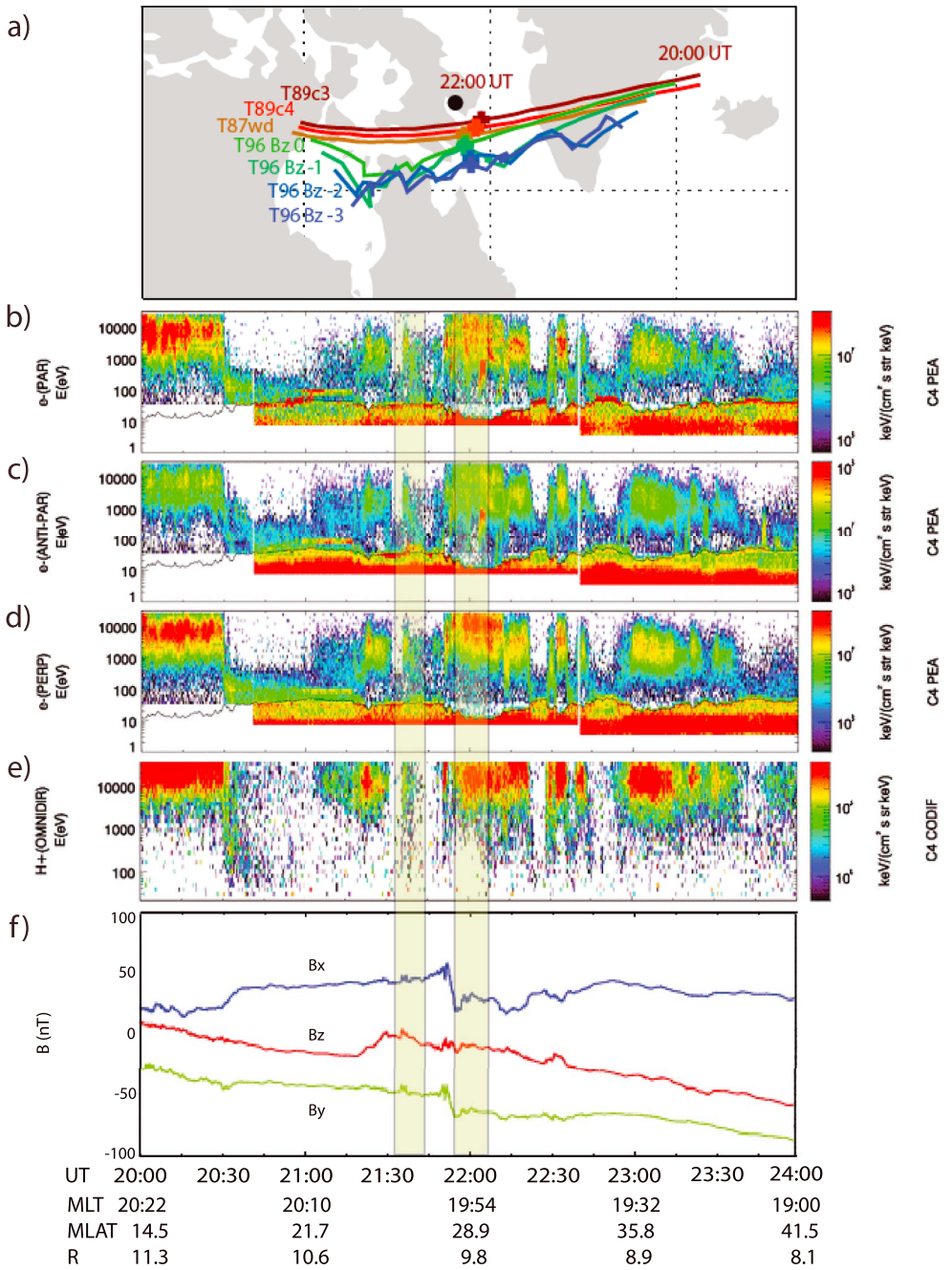

Figure 11. (a) The mapped Northern Hemisphere ground track of Cluster 4 from 2000 to 2400 UT 9 October 2015, using the seven magnetic field models provided by SSCWeb and described in the text. The crosses in each colored trace show the magnetic foot point at 2200 UT using those models. The location of Pangnirtung is indicated by the black circle. Panels (b)–(d) show the differential energy flux of electrons measured by the Plasma Electron and Current Experiment instrument as a function of energy in directions parallel (panel a), antiparallel (panel b), and perpendicular (panel c) to the local magnetic field. Panel (e) shows the omnidirectional differential energy flux of protons measured by the CIS Composition and Distribution Ion Function analyzer (CODIF) instrument as a function of energy, and panel (f) shows the three components of the magnetic field measured by the Fluxgate Magnetometer instrument, in geocentric solar ecliptic coordinates.

surge and auroral forms elongated in the north-south direction (auroral streamers) that propagated westward along the center of the electrojet.

Murphy et al. (2013), using the AMPERE constellation of low-altitude spacecraft as well as auroral imagers and multiple ground-based magnetometers, found a complex system of upward and downward field-aligned currents forms on the nightside following substorm expansion-phase onset and noted that Iijima and Potemra (1978) had much earlier found that during very active conditions, when the westward auroral electrojet had intruded deeply into the evening sector, Triad magnetometer data indicated the presence of complex field-aligned currents in that sector.

Solovyev et al. (2000) found an association between auroral brightenings and spatial distortions of auroral forms (with wavelike and vortex structures) during pseudobreakups and substorm expansion-phase events. The southward perturbations in the H (north-south) component of the magnetic field at Kotelny, Siberia (69.7 MLAT) shown in their Figure 2, associated with a ~500 km northward auroral expansion, closely resembled the typical nighttime solitary perturbation events shown in Paper 1. Similarly, Apatenkov et al. (2004) and Belakhovsky et al. (2018) both noted an association between perturbation events and vortical current structures, and Huttunen et al. (2002) found that during the April 2000 magnetic storm geomagnetically induced currents were strongly enhanced during several periods. While some perturbation intervals were associated with substorm onsets or electrojet enhancements, Huttunen et al. (2002) found that others were caused by extremely localized and short-lived electrojet activations.

4.2. Connections to Magnetotail Dynamics

Transient flows in the magnetotail have been studied for many years. Large-scale injection fronts in the magnetotail were noted by Moore et al. (1981), and more short-lived high-speed flows, denoted bursty bulk flows (BBFs) by Angelopoulos et al. (1992), were first reported by Baumjohann et al. (1990). Liu et al. (2014) reported that each BBF may contain several dipolarizing flux bundles (DFBs), defined as localized <1-min enhancements in the northward magnetic field, and rapid flux transport events, defined as intervals of high electric field (Tu et al., 2000). The leading edge of a DFB has been defined as a dipolarization front (Nakamura et al., 2002).

Many studies have found a close relation between expansion-phase auroral streamers and poleward boundary intensifications (PBIs) observed in the ionosphere and disturbances in the magnetotail; a representative sample includes Henderson et al. (1998), Sergeev et al. (1999), Kauristie et al. (2000), Zesta et al. (2000, 2006), Nishimura et al. (2012), and Lyons et al. (2012). Henderson et al. (1998) provided evidence that auroral streamers observed during the expansion and early recovery phases of substorms are an auroral manifestation of BBFs. Sergeev et al. (1999) found that sporadic earthward-directed velocity dispersed ion beams correlated with intensifications of westward current and auroral activations at the poleward edge of the auroral bulge. Kauristie et al. (2000) found an association between transient plasma sheet flows and vortex-like spatial distributions of equivalent currents deduced from ground magnetometer observations in northern Scandinavia.

Zesta et al. (2000, 2006) found that PBIs correlated well with plasma sheet fast flows observed within the same local time sector, and Nishimura et al. (2012) documented a close connection between substorm Pi2 events, expansion-phase auroral intensifications near the poleward edge of the auroral bulge, auroral streamers, and plasma sheet flow bursts. Lyons et al. (2012) investigated several large plasma sheet dipolarization fronts identified by Runov et al. (2009, 2011) and found that many of these events occurred during the substorm expansion phase after onset and were related to auroral streamers. They also noted that the auroral zone ground magnetic field showed only modest responses to substorm onsets, but abrupt, large responses to postonset dipolarization-front-related streamers, consistent with the observations reported here.

5. Summary

Observations from magnetometer arrays in Eastern Arctic Canada provide significant details on the varieties of spatial and temporal evolution of nighttime magnetic perturbation events at high latitudes. The addition of auroral images and data from high-altitude spacecraft located at near magnetically conjugate locations in the magnetotail makes it possible to connect these events to other ionospheric and magnetospheric phenomena. The following points summarize our observations:

1. None of the cases shown here occurred during the main phase of a geomagnetic storm, and only the first during the early recovery phase (of a moderate storm). Each of the three intervals of magnetic perturbations within each case occurred when the SME index was enhanced and within 1 hr of a substorm onset and a dipolarization at GOES 13, but none of the perturbations showed a close or consistent temporal relation to the onset or the dipolarization.
2. Paper 1 investigates the timing between perturbation event occurrence and substorms and magnetic storms in more detail, indicating that although most nighttime events in this high-latitude region during 2015 occurred during magnetic storms or after substorm onsets, some occurred during otherwise geomagnetically quiet periods hours or even days after the last prior substorm. Preliminary comparisons of substorm-related and nonsubstorm-related events reveal very similar levels of SYM/H and SME indices but little or no evidence of dipolarizations at synchronous orbit during nonsubstorm-related events. These comparisons will be the focus of a subsequent study.
3. The event intervals in each case showed a spatial progression, in that successive intervals occurred later at the more western and northern stations.
4. The interstation timing of individual magnetic perturbations varied. During several event intervals, peak ΔBx impulses occurred nearly simultaneously (within 1–2 min) at several stations, while during others the impulses occurred later at more northern and western stations, and during one interval they occurred later at southern stations.
5. SECs maps based on data from a wider spatial range of magnetometers North America and Greenland showed regions of large horizontal derivatives localized to within half-maximum radii of ~275 km. These regions coincided with the locations of magnetometers with large magnetic perturbations and peak derivatives.
6. GOES 13 observed one or more dipolarizations in each case and Cluster during the third case, indicating that these magnetic perturbation events were generally related to earthward flow bursts from the tail that were able to penetrate to the near-Earth plasma sheet.
7. During both of the cases for which auroral images were available, magnetic activity was generally associated with westward traveling surges, and the largest impulses were closely connected to poleward auroral expansions and/or PBIs. The magnetic perturbation events seen at Repulse Bay during these cases were coincident in time with overhead auroral streamers.

Taken together, these observations are consistent with several earlier studies connecting nighttime magnetic perturbation events not only to westward traveling surges but also to much more localized poleward boundary expansions and auroral streamers, which in turn are connected with BBFs in the tail and their associated DFBs and dipolarization fronts. These observations may prove useful in constraining efforts to identify the physical mechanism or mechanisms that produce these events and their associated geomagnetically-induced currents. In particular, the coincidence with overhead auroral streamers, the 5- to 10-min time scale, and the ~275-km effective radius of individual events may help distinguish temporal from spatial aspects of these complex events.

Acknowledgments
This work was supported by NSF Grant AGS-1651263 to Augsburg University; NSF Grant AGS-1654044 to the University of Michigan; NASA Grants 80NSSC18K0570 and 80NSSC18K1220, NASA Contract NAS5-02099, NSF Grant 1401822, and AFOSR FA9559-16-1-0364 to UCLA; NASA Grants NNX17AL22G and 80NSSC18K0657 and NSF Grant AGS-1737823 to Boston University; NSF Grant PLR-1744828 to Virginia Tech; and NASA Grant NNX16AG74G and NSF Grant 1502700 to JHU/APL. MACCS magnetometer data are available online (http://space.augsburg.edu/maccs/requestdatafile.jsp), AUTUMNX magnetometer data are available in IAGA 2002 ASCII format (http://autumn.athabascau.ca/autumnxquery2.php?year=2015&mon=01&day=01), and CANMOS magnetometer data, provided by the Geological Survey of Canada, are available in IAGA 2002 ASCII format (http://geomag.nrcan.gc.ca/data-donnee/sd-en.php). CARISMA magnetometer data are available in ASCII format (http://www.carisma.ca/carisma-data-repository), and South Pole Station magnetometer data are available in ASCII format (https://antarcticgeospace.njit.edu/Data/). AALPIP magnetometer data are available in CDF and IDL save set formats (http://mist.nianet.org/). GOES magnetometer data are available online (https://satdat.ngdc.noaa.gov/sem/goes/data/full/). Solar wind and IMF data are available at the Goddard Space Flight Center Space Physics Data Facility (https://cdaweb.sci.gsfc.nasa.gov/index.html/), as are also data from the Greenland coastal magnetometer chain. THEMIS Auroral Imager data are available at the website (http://themis.ssl.berkeley.edu). Cluster data are available at the Cluster Science Archive (https://www.cosmos.esa.int/web/csa), and the magnetic foot point of Cluster was determined using tools provided by SSCWEB (https://sscweb.gsfc.nasa.gov/). The SME index is available from SuperMAG (http://supermag.jhuapl.edu/indices/), Principal Investigator Jesper Gjerloev, derived from magnetometer data from Intermagnet; USGS, Jeffrey J. Love; CARISMA, PI Ian Mann; CANMOS, Geomagnetism Unit of the Geological Survey of Canada; The S-RAMP Database, PI K. Yumoto and Dr. K. Shiokawa; The SPIDR database; AARI, PI Oleg Troshichev; The MACCS program, PI M. Engebretson; GIMA; MEASURE, UCLA IGPP and Florida Institute of Technology; SAMBA, PI Eftyhia Zesta; 210 Chain, PI K. Yumoto; SAMNET, PI Farideh Honary; The institutes who maintain the IMAGE magnetometer array, PI Eija

References

Amm, O., Janhunen, P., Kauristie, K., Opgenoorth, H. J., Pulkkinen, T. I., & Viljanen, A. (2001). Mesoscale ionospheric electrodynamics observed with the MIRACLE network: 1. Analysis of a pseudobreakup spiral. *Journal of Geophysical Research*, *106*, 24,675–24,690. https://doi.org/10.1029/2001JA900072

Amm, O., & Viljanen, A. (1999). Ionospheric disturbance magnetic field continuation from the ground to the ionosphere using spherical elementary currents systems. *Earth Planets Space*, *51*, 431–440.

Angelopoulos, V., Baumjohann, W., Kennel, C. F., Coroniti, F. V., Kivelson, M. G., Pellat, R., et al. (1992). Bursty bulk flows in the inner central plasma sheet. *Journal of Geophysical Research*, *97*, 4027–4039. https://doi.org/10.1029/91JA02701

Apatenkov, S. V., Sergeev, V. A., Pirjola, R., & Viljanen, A. (2004). Evaluation of the geometry of ionospheric current systems related to rapid geomagnetic variations. *Annals of Geophysics*, *22*, 63–72. https://doi.org/10.5194/angeo-22-63-2004

Balogh, A., Carr, C. M., Acuña, M. H., Dunlop, M. W., Beek, T. J., Brown, P., et al. (2001). The Cluster magnetic field investigation: Overview of in-flight performance and initial results. *Annals of Geophysics*, *19*, 1207–1217. https://doi.org/10.5194/angeo-19-1207-2001

Baumjohann, W., Paschmann, G., & Lühr, H. (1990). Characteristics of high-speed flows in the plasma sheet. *Journal of Geophysical Research*, *95*, 3801–3809. https://doi.org/10.1029/JA095iA04p03801

Belakhovsky, V. B., Pilipenko, V. A., Sakharov, Y. A., & Selivanov, V. N. (2018). Characteristics of the variability of a geomagnetic field for studying the impact of the magnetic storms and substorms on electrical energy systems. *Izvestiya, Physics of the Solid Earth*, *54*, 52–65.

Tanskanen; PENGUIN; AUTUMN, PI Martin Connors; DTU Space, PI Dr. Rico Behlke; South Pole and McMurdo Magnetometer, PIs Louis J. Lanzerotti and Allan T. Weatherwax; ICESTAR; RAPIDMAG; PENGUIn; British Artarctic Survey; McMAC, PI Dr. Peter Chi; BGS, PI Dr. Susan Macmillan; Pushkov Institute of Terrestrial Magnetism, Ionosphere and Radio Wave Propagation (IZMIRAN); GFZ, PI Dr. Juergen Matzka; MFGI, PI B. Heilig; IGFPAS, PI J. Reda; and University of L'Aquila, PI M. Vellante.

Clauer, C. R., Kim, H., Deshpande, K., Xu, Z., Weimer, D., Musko, S., et al. (2014). An autonomous adaptive low-power instrument platform (AAL-PIP) for remote high-latitude geospace data collection. *Geoscientific Instrumentation, Methods and Data Systems*, *3*, 211–227. https://doi.org/10.5194/gi-3-211-2014

Connors, M., Schofield, I., Reiter, K., Chi, P. J., Rowe, K. M., & Russell, C. T. (2016). The AUTUMNX magnetometer meridian chain in Québec, Canada. *Earth, Planets and Space*, *68*, 2. https://doi.org/10.1186/s40623-015-0354-4

Dimmock, A. P., Rosenqvist, L., Hall, J.-O., Viljanen, A., Yordanova, E., Honkonen, I., et al. (2019). The GIC and geomagnetic response over Fennoscandia to the 7-8 September 2017 geomagnetic storm. *Space Weather*, *17*, 989–1010. https://doi.org/10.1029/2018SW002132

Engebretson, M. J., Hughes, W. J., Alford, J. L., Zesta, E., Cahill, L. J. Jr., Arnoldy, R. L., & Reeves, G. D. (1995). Magnetometer array for cusp and cleft studies observations of the spatial extent of broadband ULF magnetic pulsations at cusp/cleft latitudes. *Journal of Geophysical Research*, *100*, 19,371–19,386. https://doi.org/10.1029/95JA00768

Engebretson, M. J., Pilipenko, V. A., Ahmed, L. Y., Posch, J. L., Steinmetz, E. S., Moldwin, M. B., et al. (2019). Nighttime magnetic perturbation events observed in Arctic Canada: 1. Survey and statistical analysis. *Journal of Geophysical Research: Space Physics*, *124*. https://doi.org/10.1029/2019JA026794

Engebretson, M. J., Araki, T., Arnoldy, R. L., Carpenter, D. L., Doolittle, J. H., Fukunishi, H., et al. (1997). The United States automatic geophysical observatory (AGO) program in Antarctica. In M. Lockwood, M. N. Wild, & H. J. Opgenoorth (Eds.), *the Satellite—Ground Based Coordination Sourcebook, ESA-SP-1198* (pp. 65–99). ESTEC, Noordwijk, Netherlands: ESA Publications.

Henderson, M. G., Reeves, G. D., & Murphree, J. S. (1998). Are north-south aligned auroral structures an ionospheric manifestation of bursty bulk flows? *Geophysical Research Letters*, *25*, 3737–3740. https://doi.org/10.1029/98GL02692

Huttunen, K. E. J., Koskinen, H. E. J., Pulkkinen, T. I., Pulkkinen, A., Palmroth, M., Reeves, E. G. D., & Singer, H. J. (2002). April 2000 magnetic storm: Solar wind driver and magnetospheric response. *Journal of Geophysical Research*, *107*(A12), 1440. https://doi.org/10.1029/2001JA009154

Iijima, T., & Potemra, T. A. (1978). Large-scale characteristics of field-aligned currents associated with substorms. *Journal of Geophysical Research*, *83*, 599–615. https://doi.org/10.1029/JA083iA02p00599

Johnstone, A. D., Alsop, C., Burge, S., Carter, P. J., Coates, A. J., Coker, A. J., et al. (1997). Peace: A plasma electron and current experiment. *Space Science Reviews*, *79*, 351–398. https://doi.org/10.1023/A1004938001388

Kauristie, K., Sergeev, V. A., Kubyshkina, M., Pulkkinen, T. I., Angelopoulos, V., Phan, T., et al. (2000). Ionospheric current signatures of transient plasma sheet flows. *Journal of Geophysical Research*, *105*, 10,677–10,690. https://doi.org/10.1029/1999JA900487

Kistler, L. M., Mouikis, C. G., Cao, X., Frey, H., Klecker, B., Dandouras, I., et al. (2006). Ion composition and pressure changes in storm time and nonstorm substorms in the vicinity of the near-Earth neutral line. *Journal of Geophysical Research*, *111*, A11222. https://doi.org/10.1029/2006JA011939

Kozyreva, O. V., Pilipenko, V. A., Belakhovsky, V. B., & Sakharov, Y. A. (2018). Ground geomagnetic field and GIC response to March 17, 2015 storm. *Earth, Planets, and Space*, *70*. https://doi.org/10.1186/s40623-018-0933-2

Liu, J., Angelopoulos, V., Zhou, X.-Z., & Runov, A. (2014). Magnetic flux transport by dipolarizing flux bundles. *Journal of Geophysical Research: Space Physics*, *119*, 909–926. https://doi.org/10.1002/2013JA019395

Liu, Y., Kistler, L. M., Mouikis, C. G., Klecker, B., & Dandouras, I. (2013). Heavy ion effects on substorm loading and unloading in the Earth's magnetotail. *Journal of Geophysical Research: Space Physics*, *118*, 2101–2112. https://doi.org/10.1002/jgra.50240

Lühr, H., Aylward, A., Buchert, S. C., Pajunpää, A., Pajunpää, K., Holmboe, T., & Zalewski, S. M. (1998). Westward moving dynamic substorm features observed with the IMAGE magnetometer network and other ground-based instruments. *Annales Geophysicae*, *16*, 425–440. https://doi.org/10.1007/s00585-998-0425-y

Lyons, L. R., Nishimura, Y., Donovan, E., & Angelopoulos, V. (2013). Distinction between auroral substorm onset and traditional ground magnetic onset signatures. *Journal of Geophysical Research: Space Physics*, *118*, 4080–4092. https://doi.org/10.1002/jgra.50384

Lyons, L. R., Nishimura, Y., Xing, X., Runov, A., Angelopoulos, V., Donovan, E., & Kikuchi, T. (2012). Coupling of dipolarization front flow bursts to substorm expansion phase phenomena within the magnetosphere and ionosphere. *Journal of Geophysical Research*, *117*, A02212. https://doi.org/10.1029/2011JA017265

Mann, I. R., Milling, D. K., Rae, I. J., Ozeke, L. G., Kale, A., Kale, Z. C., et al. (2008). The upgraded CARISMA magnetometer array in the THEMIS era. *Space Science Reviews*, *141*(1-4), 413–451. https://doi.org/10.1007/s11214-008-9457-6

Mende, S. B., Harris, S. E., Frey, H. U., Angelopoulos, V., Russell, C. T., Donovan, E., et al. (2008). The THEMIS array of ground-based observatories for the study of auroral substorms. *Space Science Reviews*, *141*, 357. https://doi.org/10.1007/s11214-008-9380-x

Moore, T., Arnoldy, R., Feynman, J., & Hardy, D. (1981). Propagating substorm injection fronts. *Journal of Geophysical Research*, *86*, 6713–6726. https://doi.org/10.1029/JA086iA08p06713

Murphy, K. R., Mann, I. R., Rae, I. J., Waters, C. L., Frey, H. U., Kale, A., et al. (2013). The detailed spatial structure of field-aligned currents comprising the substorm current wedge. *Journal of Geophysical Research: Space Physics*, *118*, 7714–7727. https://doi.org/10.1002/2013JA018979

Nakamura, R., Baumjohann, W., Klecker, B., Bogdanova, Y., Balogh, A., Rème, H., et al. (2002). Motion of the dipolarization front during a flow burst event observed by Cluster. *Geophysical Research Letters*, *29*(20), 1942. https://doi.org/10.1029/2002GL015763

Newell, P. T., & Gjerloev, J. W. (2011). Evaluation of SuperMAG auroral electrojet indices as indicators of substorms and auroral power. *Journal of Geophysical Research*, *116*, A12211. https://doi.org/10.1029/2011JA016779

Ngwira, C. M., Pulkkinen, A. A., Bernabeu, E., Eichner, J., Viljanen, A., & Crowley, G. (2015). Characteristics of extreme geoelectric fields and their possible causes: Localized peak enhancements. *Geophysical Research Letters*, *42*, 6916–6921. https://doi.org/10.1002/2015GL065061

Ngwira, C. M., Sibeck, D. G., Silveira, M. D. V., Georgiou, M., Weygand, J. M., Nishimura, Y., & Hampton, D. (2018). A study of intense local d*B*d*t* variations during two geomagnetic storms. *Space Weather*, *16*, 676–693. https://doi.org/10.1029/2018SW001911

Nikitina, L., Trichtchenko, L., & Boteler, D. H. (2016). Assessment of extreme values in geomagnetic and geoelectric field variations for Canada. *Space Weather*, *14*, 481–494. https://doi.org/10.1002/2016SW001386

Nishimura, Y., Lyons, L. R., Kikuchi, T., Angelopoulos, V., Donovan, E., Mende, S., et al. (2012). Formation of substorm Pi2: A coherent response to auroral streamers and currents. *Journal of Geophysical Research*, *117*, A09218. https://doi.org/10.1029/2012JA017889

Pulkkinen, A., Thomson, A., Clarke, E., & McKay, A. (2003). April 2000 geomagnetic storm: Ionospheric drivers of large geomagnetically induced currents. *Annales Geophysicae*, *21*(3), 709–717. https://doi.org/10.5194/angeo-21-709-2003

Rème, H., Aoustin, C., Bosqued, J. M., Dandouras, I., Lavraud, B., Sauvaud, J. A., et al. (2001). First multispacecraft ion measurements in and near the Earth's magnetosphere with the identical Cluster ion spectrometry (CIS) experiment. *Annals of Geophysics*, *19*(10/12), 1303–1354. https://doi.org/10.5194/angeo-19-1303-2001

Runov, A., Angelopoulos, V., Sitnov, M. I., Sergeev, V. A., Bonnell, J., McFadden, J. P., et al. (2009). THEMIS observations of an earthward-propagating dipolarization front. *Geophysical Research Letters*, *36*, L14106. https://doi.org/10.1029/2009GL038980

Runov, A., Angelopoulos, V., Zhou, X.-Z., Zhang, X.-J., Li, S., Plaschke, F., & Bonnell, J. (2011). A THEMIS multicase study of dipolarization fronts in the magnetotail plasma sheet. *Journal of Geophysical Research*, *116*, A05216. https://doi.org/10.1029/2010JA016316

Sergeev, V. A., Liou, K., Meng, C.-I., Newell, P. T., Brittnacher, M., Parks, G., & Reeves, G. D. (1999). Development of auroral streamers in association with localized impulsive injections to the inner magnetotail. *Geophysical Research Letters*, *26*, 417–420. https://doi.org/10.1029/1998GL900311

Singer, H. J., Matheson, L., Grubb, R., Newman, A., & Bouwer, S. D. (1996). Monitoring space weather with the GOES magnetometers, in SPIE Conference Proceedings, vol. 2812, edited by E. R. Washwell, pp. 299–308, GOES-8 and Beyond SPIE, Bellingham, Wash.

Solovyev, S. I., Baishev, D. G., Barkova, E. S., Molochushkin, N. E., & Yumoto, K. (2000). Pi2 magnetic pulsations as response on spatio-temporal oscillations of auroral arc current system. *Geophysical Research Letters*, *27*, 1839–1842. https://doi.org/10.1029/2000GL000037

Tsyganenko, N. A. (1987). Global quantitative models of the geomagnetic field in the cislunar magnetosphere for different disturbance levels. *Planetary and Space Science*, *35*, 1347–1358. https://doi.org/10.1016/0032-0633(87)90046-8

Tsyganenko, N. A. (1989). A magnetospheric magnetic field model with a warped tail current sheet. *Planetary and Space Science*, *37*(1), 5–20. https://doi.org/10.1016/0032-0633(89)90066-4

Tsyganenko, N. A. (1996). Effects of the solar wind conditions on the global magnetospheric configuration as deduced from data-based field models, in Proceedings of the ICS-3 Conference on Substorms, Eur. Space Agency Spec. Publ., ESA SP-389, 181.

Tu, J.-N., Tsuruda, K., Hayakawa, H., Matsuoka, A., Mukai, T., Nagano, I., & Yagitani, S. (2000). Statistical nature of impulsive electric fields associated with fast ion flow in the near-Earth plasma sheet. *Journal of Geophysical Research*, *105*, 18,901. https://doi.org/10.1029/1999JA000428

Viljanen, A. (1997). The relation between geomagnetic variations and their time derivatives and implications for estimation of induction risks. *Geophysical Research Letters*, *24*, 631–634. https://doi.org/10.1029/97GL00538

Weygand, J. M., Amm, O., Viljanen, A., Angelopoulos, V., Murr, D., Engebretson, M. J., et al. (2011). Application and validation of the spherical elementary currents systems technique for deriving ionospheric equivalent currents with the North American and Greenland ground magnetometer arrays. *Journal of Geophysical Research*, *116*, A03305. https://doi.org/10.1029/2010JA06177

Zesta, E., Lyons, L., & Donovan, E. (2000). The auroral signature of Earthward flow bursts observed in the magnetotail. *Geophysical Research Letters*, *27*, 3241–3244. https://doi.org/10.1029/2000GL000027

Zesta, E., Lyons, L., Wang, C.-P., Donovan, E., Frey, H., & Nagai, T. (2006). Auroral poleward boundary intensifications (PBIs): Their two-dimensional structure and associated dynamics in the plasma sheet. *Journal of Geophysical Research*, *111*, A05201. https://doi.org/10.1029/2004JA010640